Development of an Aeroelastic Stability Boundary for a Rotor in Autorotation

J Trchalík*, Dr E A Gillies†, Dr D G Thomson‡

* PhD Research Student
email: jtrchali@aero.gla.ac.uk

† Senior Lecturer,
email: ericg@aero.gla.ac.uk

‡ Senior Lecturer,
email: d.thomson@aero.gla.ac.uk

Tel.: +44 141 330 3575
Fax: +44 141 330 5560

Department of Aerospace Engineering
University of Glasgow
Glasgow, G12 8QQ
Scotland

Keywords - autogyro, aeroelasticity, rotor, rotor blade, rotorcraft, stability, axial flight, forward flight, FEM, MATLAB

January 9, 2008

Abstract

For the present study, a mathematical model *AMRA* was created to simulate the aeroelastic behaviour of a rotor during autorotation. Our model: *Aeroelastic Model of a Rotor in Autorotation* (AMRA) captures transverse bending and teeter, torsional twist and lag-wise motion of the rotor blade and hence it is used to investigate couplings between blade flapping, torsion and rotor speed. Lagrange's method was used for the modelling of blade flapping and chord-wise bending. Torsional twist of the rotor blade was modelled with the aid of finite element method (FEM), and blade transverse bending could also be modelled in FEM. The model can switch between using a full FEM model for bending and torsion, or a FEM model for torsion and simple blade teeter, depending on the complexity that the user requires.

The AMRA model was verified against experimental data obtained during a CAA sponsored flight test programme of the G-UNIV autogyro. Published results of modal analysis of helicopter rotor blades and other data published in open literature were used to validate the FEM model of the rotor blade. The first torsional natural frequency of the 'McCutcheon' rotor blades was measured with the aid of high-speed camera and used for validation of the FEM model of blade torsional twist. As a further verification of the modelling method, Aérospatiale Puma helicopter rotor blade data were compared on a Southwell plot showing comparison between experimental results and AMRA estimation.

The aeromechanical behaviour of the rotor during both axial flight and forward flight in autorotation was investigated. A significant part of the research was focused on investigation of the effect of different values of torsional and flexural stiffness, and the relative positions of blade shear centre/elastic axis and centre of mass of the blade on stability during the autorotation.

Presented at the AHS Specialist's Conference on Aeromechanics, San Francisco, CA, Jan. 23-25, 2008.

The results obtained with the aid of the model demonstrate the interesting, and unique, characteristics of the autorotative regime - with instabilities possible in bending and torsion, but also in rotorspeed. Coupled rotor speed/flap/twist oscillations (flutter and divergence) occur if the torsional stiffness of the blade is lower than a critical value, or if the blade centre of mass is significantly aft of the blade twisting axis, as is the case in helicopter pitch-flap flutter. The instability shown here, however, is *specific* to the autogyro, or autorotating rotor, as it *is coupled with rotorspeed*, and so differs from both helicopter rotor flutter and fixed-wing flutter. The coupling with rotorspeed allows a combined flutter and divergence instability, where the rotor begins to flutter in rotorspeed, teeter angle and torsional twist and, once the rotorspeed had dropped below a critical value, then moves into divergence in flap and rotorspeed. It was found that the aeroelastic behaviour of a rotor in autorotation is significantly affected by the strong coupling of blade bending stiffness and teeter angle with rotorspeed, and the strong coupling between blade aeroelastic twist and rotor torque.

Nomenclature

$[\Lambda]$	Dynamic inflow static gain matrix [-]
$[\tau]$	Time constant matrix [-]
α_D	Angle of attack of the rotor disk [rad]
χ	Wake skew angle, $\chi \approx \arctan \frac{\mu_x}{\lambda}$ [rad]
γ	Angle of climb of the vehicle [rad]
$\hat{\alpha}$	Parameter of mass matrix of blade bending FEM [1]
$\hat{\mu}$	Blade weight per length [kg/m]
$\hat{w}$	Test (weighting) function [1]
ι	Rotor disk longitudinal tilt, i.e. angle between rotor disk plane and horizontal plane [rad]
μ_x	Advance ratio defined parallel to rotor disk plane, $\mu_x = \frac{\sqrt{V_x+V_y}}{\Omega R}$ [1]
μ_z	Advance ratio defined perpendicular to rotor disk plane, $\mu_z = \frac{V_z}{\Omega R} = \lambda - \lambda_i$ [1]
$\{A_B\}$	Sum of additional flexural forcing terms [N]
$\{A_T\}$	Sum of additional torsional forcing terms [N]
C_0	Apparent mass factor, $C_0 = 1$ for Pitt-Peters dynamic inflow model [1]
H	Blade shape function [1]
l_i	Length of i-th rotor blade element, $l_i = r_{i+1} - r_i$ [m]
N_{elem}	Number of blade span-wise elements [1]
q	Torsional aerodynamic loading per length [N]
t	Blade thrust per length [N/m]
u_m	Mass flow parameter [1]
v_t	Total velocity at the rotor disk centre [m/s]
v_{ic}	Longitudinal component of induced velocity [m/s]
v_{is}	Lateral component of induced velocity [m/s]
x_i	Span-wise dimensionless coordinate of i-th rotor blade node, $r_i = Rx_i$ [m]

1. Introduction

The autogyro represents the first successful rotorcraft design and it paved the way for the development of the helicopter during the 1940s. Further development of the autogyro was ceased during the following decades as helicopters became more successful. Interest in the autogyro as a recreational vehicle was resurrected in recent years thanks to simplicity of its design and low operational costs. Its wider use in military and civil applications is also currently under investigation.

Autogyros use two-bladed teetering rotors for generation of lift. Unlike in helicopters, the rotor is not powered by an engine but rotor torque is generated by the aerodynamic forces and the rotor has to be pre-rotated before take-off. Autogyros do not need a tail rotor as there is no torque acting on their fuselage. Longitudinal and lateral tilt of the rotor disk is used for longitudinal and lateral control of the vehicle. Most of autogyros use the combination of two-stroke or four-stroke engine and a propeller in pusher configuration, for thrust.

Unfortunately, autogyros in the UK have been involved in number of fatal accidents during the last two decades.[1] Very little data on autogyro flight mechanics and handling qualities were available in the literature at the time, which led the *UK Civil Aviation Authority* (CAA) and the Department of Aerospace Engineering, University of Glasgow, to investigate the aerodynamics and flight mechanics of an autogyro.[1–4] The

cause of some of these accidents still remains unclear and rotor aeroelasticity has not yet been investigated as a contributing factor. The aeroelastic behaviour of a rotor in autorotation is a relatively unexplored problem, and the aim of this investigation is to identify flight conditions or configurations of the rotor that might cause instabilities, and explore the effects of aeroelasticity on flight mechanics models of autogyros.

2. Aeroelastic Model of a Rotor in Autorotation (*AMRA*)

There are substantial differences between the aerodynamics of a helicopter rotor and of a rotor in autorotation. During autorotation, both torque and thrust are generated exclusively by flow through the rotor disc, thus the rotor has one extra degree of freedom. Thrust and torque are functions of rotor speed and distribution of local angles of attack along the blade span. Further, angles of attack are dependent upon blade twist, rotor speed, speed of descent and induced velocity. It can be easily shown that both speed of descent and rotor angular velocity are strongly dependent upon rotor torque and rotor thrust. This makes modelling of rotor aeromechanics during autorotation relatively challenging.

During steady autorotation, the overall torque generated by flow through the rotor disc balances the profile drag and rotor thrust is equal to the weight of the vehicle.[5,6] There are several design parameters of the rotor that determine whether steady autorotation is possible. The most important are blade incidence angle (i.e. angle of attack of the blade relative to the rotor disc plane) and blade torsional stiffness. Torque equilibrium can not be achieved for high incidence angles due to the high value of blade drag. If torsional rigidity is too low, extensive blade twist has the same effect. The extra degree of freedom in rotor speed has significant implication for autogyro rotor stability. Decrement of the rotor speed decreases centrifugal stiffness of the rotor and the resulting higher deflections in flap and twist generate more drag and may cause further drop in rotor speed.

The *AMRA* model was developed with the aid of MATLAB programming language. A blade element method combined with quasi-steady or unsteady aerodynamics (Theodorsen's theory) is used for calculation of aerodynamic forces and moments generated by the rotor blade. Two rotor blades and arbitrary number of blade span-wise elements can be used. The aerodynamic characteristics of the aerofoil for the full range of angles of attack are approximated with the aid of wind tunnel data.[7] A NACA 0012 aerofoil was chosen for the first version of the *AMRA* model since aerodynamic characteristics for the full range of angles of attack of the aerofoil are available.[8] A semi-empirical method of induced velocity calculation was used in the first versions of the *AMRA* model. The original calculation[9] was improved in order to capture blade stall and compressibility of the airflow. A simplified version of Peters - HaQuang inflow model modified by Houston and Brown[2] replaced semi-empirical approach in the later versions of the *AMRA* model in order to improve fidelity of forward flight simulations.

Lagrangian equations of motion were used to describe dynamics of the rotor blade. Chordwise locations of elastic axis (EA), centre of gravity (CG) and aerodynamic centre (AC) can be set in each span-wise station. Values of flexural and torsional rigidity of the blade can be set to investigate the behaviour of the rotor for different physical properties of the blades. The *AMRA* model also allows placement of single concentrated mass at any span-wise station of the blade.

2.1. Modelling of Rotor Aerodynamics in Autorotation

The blade element method represents a widely used tool for description of the flow through a rotor disc. The theory has to be modified in order to capture the aerodynamics of a rotor in autorotation. During autorotation, the flow through the rotor has the opposite direction that in the case of powered flight of a helicopter. Hence the blade aerodynamic angle of attack can has to be expressed as[9–12]

$$\alpha = \phi + \theta \tag{1}$$

Since autogyros use longitudinal and lateral rotor disk tilt for control, equations describing inflow velocity components have to be modified too. Inflow velocity is a function of angle of attack of the rotor disc that is given by sum of incidence angle of the rotor disc (i.e. angle between rotor disc plane and the horizontal plane) and pitch angle of the vehicle (see equation 2). Rotor disc angle of attack is 90deg during axial flight.

$$\begin{aligned} \alpha_D &= \iota + \gamma \\ \gamma &= atan\left(\frac{V_d}{V_h}\right) \end{aligned} \tag{2}$$

An assumption of a linear lift curve and parabolic drag curve is often used in order to simplify the model and speed up computations. However, this approach does not allow the effects of blade stall, drag divergence and most importantly air compressibility to be captured. Since the aerodynamic characteristics of rotor blade elements depend upon local values of angle of attack and Mach number, it is convenient to express aerodynamic characteristics of the blade airfoil as functions of these two variables. This can be achieved by expressing aerodynamic characteristics of the blade in terms of polynomial functions of angle of attack and Mach number.[5]

It was shown by Prouty[7] that it is possible to obtain full-range angle of attack aerodynamic data of an airfoil with the aid of polynomial fit. Prouty uses the example of the NACA 0012 airfoil in his book[7]. Prouty's empirical equations were derived from data published in Carpenter[13]. Since full-range AOA aerodynamic data for the same airfoil are available from numerous sources[8,14], Prouty's approach was amended and incorporated into the *AMRA* model.

2.2. Modelling of Dynamic Inflow During Autorotation

Dynamic inflow models developed by Pitt and Peters, Gaonkar and Peters, Peters and HaQuang and Peters and He represent one of the most popular dynamic inflow models. Modern three-state dynamic inflow models can be defined in the following form[15,16]

$$[\tau]\begin{bmatrix}\dot{v}_{i0}\\ \dot{v}_{is}\\ \dot{v}_{ic}\end{bmatrix}+\begin{bmatrix}v_{i0}\\ v_{is}\\ v_{ic}\end{bmatrix}=[\Lambda]\begin{bmatrix}T\\ L_R\\ M_R\end{bmatrix} \tag{3}$$

Peters - HaQuang inflow model was enhanced by Houston and Brown[17] in order to capture inflow of a rotor in autorotation. The time matrix and dynamic inflow static gain matrix can be written for a rotor in autorotative flight regime in the following form

$$[\tau]=\begin{bmatrix}\frac{4R}{3\pi v_t C_0} & 0 & \frac{-R\tan\frac{\chi}{2}}{12u_m}\\ 0 & \frac{64R}{45u_m(1+\cos\chi)} & 0\\ \frac{5R\tan\frac{\chi}{2}}{8v_t} & 0 & \frac{64R\cos\chi}{45u_m(1+\cos\chi)}\end{bmatrix} \tag{4}$$

and

$$[\Lambda]=\frac{1}{\rho\pi R^3}\begin{bmatrix}\frac{R}{2v_t} & 0 & \frac{15\pi\tan\frac{\chi}{2}}{64u_m}\\ 0 & \frac{-4}{u_m(1+\cos\chi)} & 0\\ \frac{15\pi\tan\frac{\chi}{2}}{64v_t} & 0 & \frac{-4\cos\chi}{u_m(1+\cos\chi)}\end{bmatrix} \tag{5}$$

Total induced velocity at azimuth angle ψ and radial station x then is[17]

$$v_i = v_{i0} + v_{ic}x\cos\psi + v_{is}x\sin\psi \tag{6}$$

Although a full dynamic model with three degrees of freedom was incorporated into the *AMRA*, its simplified version was used in order to reduce computational time. From the system of equations (3), only first equation is used in the simulation as the remaining two components of induced velocity can be neglected.[6,18] This modification decreases computing time and reduces complexity of the model significantly. The equation below shows solution for the rate of change of vertical component of induced velocity.

$$\dot{v}_{i0}=-\frac{3C_0\left(2\pi\rho R^2 v_{i0}\sqrt{V_x^2+V_y^2+V_z^2+\sqrt{\frac{T}{\pi\rho R^2}}\left(\frac{1}{\sqrt{2}}-\sqrt{2}V_z\right)}-T\right)}{8\rho R^3} \tag{7}$$

Matrix equation 3 then becomes

$$v_i = \int \dot{v}_{i0}dt \tag{8}$$

2.3. Rotor Blade Physical Properties

Since the majority of autogyro rotor blades are manufactured by small private companies, it is difficult to get any information on their structural properties. A pair of McCutcheon blades were subjected to a series of experiments in order to assess their physical properties and mass distribution. Data gathered during the experiments were used as input values of the simulations and also for validation of the model of rotor blade dynamics. The majority of experimental measurements and their results are described by the authors elsewhere[19]

The data obtained during the experimental measurements are summarized as follows: elastic axis position is located between 35.5% (inboard) and 27.24% (outboard) of blade chord; position of the blade inertial axis is around 30% of blade chord (inboard) and it grows to 36% towards the tip of the blade. Mass per length of the blade is 4.25kg/m in the root part of the blade and averages 2.7kg/m outboards. Torsional stiffness of the blade changes linearly along the blade span from $1534Nm^2/rad$ to $1409Nm^2/rad$. Blade flexural stiffness was estimated with the aid of measurement of first bending natural frequency of the blade. The value of transverse stiffness is $1166Nm^2$ and it was assumed it is constant along blade span.

The first torsional frequency of the rotor blade was estimated as $f_{1T} = 34.8Hz$.

3. Modelling of Rotor Blade Dynamics

The *AMRA* model can use Lagrange's equations of motion or the finite element method (FEM) for modelling of rotor blade structural dynamics in bending, teeter and torsion. Alternatively, combinations of both approaches can be used. Thus allowed comparison of differences between results obtained with the aid of models with different levels of complexity. In Lagrange's method, the blades are assumed to be perfectly rigid and blade stiffness is modelled with springs located at the root of each blade. Bending and torsional deflections are assumed to be constant along the blade span. This requires less computational time but it does not provide a full picture of the dynamics of the system since it is significantly simplified. Finite element analysis (FEA) of coupled bending-torsion of the blade on the other hand is highly complex and requires significantly higher computational time.

Lagrange's method is an elegant way of obtaining the equations of motion and it is useful for modelling of complex dynamics of rotorcraft rotor blades. In order to use of span-wise distributions of blade physical properties and also allow coupling of Lagrange's equations of motion with FEA of blade dynamics, each rotor blade is discretized into a number of lumped masses. Lagrange's equations of motion are generated for each lumped mass. Linearized and simplified versions of equations of motion for coupled torsion-flap of a rotor blade are published in the open literature[20].

Galerkin's method of solution is used in the *AMRA* model. The model can perform dynamic FEA of blade torsion or blade bending for teetering rotors. Alternatively, FEA of coupled bending-torsion dynamics with inclusion of teeter can be used. A 1D FEA was used in order to reduce complexity of the model. Each blade element has two nodes and number of degrees of freedom differs from one (torsion only) to three (torsion with flap-wise bending). Differential equation of blade torsion can be written in following form[21]

$$\frac{\partial \hat{w}}{\partial r} GJ \frac{\partial \theta}{\partial r} + \hat{w} i_x \ddot{\theta} + \hat{w} A_T - \hat{w} q = 0. \quad (9)$$

The term A_T represents sum of terms that represent the effect of coupling of blade torsional dynamics with degrees of freedom in flap and rotation.

Although solution of the differential equation of blade torsion with the aid of FEM does not require shape functions of higher order and linear shape functions can be used, cubic shape function was chosen for modelling of blade torsion in *AMRA*. Cubic shape function is defined as follows.[21]

$$\begin{aligned} H_1 &= 3\left(x_{i+1} - x\right)^2 - 2\left(x_{i+1} - x\right)^3 \\ H_2 &= 1 - H_1 = 3\left(x - x_i\right)^2 - 2\left(x - x_i\right)^3 \end{aligned} \quad (10)$$

Corresponding mass and stiffness matrices and forcing vector are as follows[21]

$$[K_i] = GJ \begin{bmatrix} \frac{-6}{5l_i} & \frac{6}{5l_i} \\ \frac{6}{5l_i} & \frac{-6}{5l_i} \end{bmatrix} \quad (11)$$

$$[M_i] = i_{x,i} \begin{bmatrix} \frac{13l_i}{35} & \frac{9l_i}{70} \\ \frac{9l_i}{70} & \frac{13l_i}{35} \end{bmatrix} \quad (12)$$

$$\{f_i\} = f_i \begin{Bmatrix} \frac{l_i}{2} \\ \frac{l_i}{2} \end{Bmatrix} \quad (13)$$

Alternatively, diagonal (or diagonally lumped) mass matrix can be used. It speeds up the computations as inversion of this mass matrix is much easier than in case of consistent mass matrix[21]

$$[M_i] = i_{x,i} \begin{bmatrix} \frac{l_i}{2} & 0 \\ 0 & \frac{l_i}{2} \end{bmatrix} \quad (14)$$

The finite element model of blade bending has two nodes per element but in contrary to the FEM model of blade torsion it requires two degrees of freedom per node - vertical displacement and flap-wise rotation. Differential equation of blade bending is shown below.[21]

$$\frac{\partial^2 \hat{w}}{\partial r^2} EI \frac{\partial^2 w}{\partial r^2} + \hat{w} \hat{\mu} \ddot{w} + \hat{w} A_B - \hat{w} t = 0 \quad (15)$$

Again, the term $A_{B,i}$ in the above equation represents a sum of all coupling terms .

Unlike FEA of blade torsion, modelling of blade bending with the aid of FEM requires shape functions of higher order. Hence, two different shape functions have to be used in order to describe distribution of both vertical displacement of blade nodes and slope of blade elements over a blade element. These shape functions are called Hamiltonian shape functions and they are based on the cubic shape function described in equation (10).[21] Application of Hamiltonian

shape functions results in the following forms of stiffness matrix, consistent mass matrix and forcing vector.[21]

$$[K_i] = \frac{EI}{l_i^3}\begin{bmatrix} 12 & 6l_i & -12 & 6l_i \\ 6l_i & 4l_i^2 & -6l_i & 2l_i^2 \\ -12 & -6l_i & 12 & -6l_i \\ 6l_i & 2l_i^2 & -6l_i & 4l_i^2 \end{bmatrix} \quad (16)$$

$$[M_i] = \mu_i \frac{l_i}{420}\begin{bmatrix} 156 & 22l_i & 54 & -13l_i \\ 22l_i & 4l_i^2 & 13l_i & -3l_i^2 \\ 54 & 13l_i & 156 & -22l_i \\ -13l_i & -3l_i^2 & -22l_i & 4l_i^2 \end{bmatrix} \quad (17)$$

$$\{f_i\} = \frac{f_i}{12}\begin{Bmatrix} 6l_i \\ l_i^2 \\ 6l_i \\ -l_i^2 \end{Bmatrix} \quad (18)$$

A diagonal form of mass matrix is more convenient for dynamic analysis. Parameter $\hat{\alpha}$ has to be a positive number smaller than $\frac{1}{50}$. Kwon *et al*[21] recommends $\hat{\alpha} = \frac{1}{78}$, which is used in *AMRA*.

$$[M_i] = \mu_i l_i \begin{bmatrix} \frac{1}{2} & 0 & 0 & 0 \\ 0 & \hat{\alpha} l_i^2 & 0 & 0 \\ 0 & 0 & \frac{1}{2} & 0 \\ 0 & 0 & 0 & \hat{\alpha} l_i^2 \end{bmatrix} \quad (19)$$

4. Verification of the *AMRA* Model

Although the *AMRA* model is fully functional standalone model of rotor aeromechanics in autorotation, its main purpose was to test model of blade dynamics in autorotation so that it can be incorporated into a rotorcraft flight mechanics model (i.e. *RASCAL*[22], *G-SIM*[23] or other). Therefore, the main objective of the validation phase of the project was to make sure that blade dynamics are computed correctly by the *AMRA* model. FEM model of blade torsion represents the key block of *AMRA* and extra care was taken during its validation. Values of teetering angle predicted by the *AMRA* model were verified against G-UNIV autogyro flight data[23]. Estimations of flight performance during flight in autorotation were also successfully compared with experimental data published in open literature.[5]

4.1. Validation of Model of Rotor Blade Teeter

Data gathered during CAA sponsored series of flight test of the University of Glasgow Montgomerie-Parsons autogyro (G-UNIV) were used for validation of model of blade teeter that is included in the *AMRA* model.

However, *AMRA* uses a NACA 0012 airfoil that has different aerodynamics characteristics in comparison with NACA 8-H-12 that are used in McCutcheon rotor blades. In order to reach similar flight conditions during simulations (i.e. rotor speed and speed of descent), rotor speed was set to mean value of rotor speed measured during the flight tests. Two different regimes of steady level flight were chosen for the validation. Predictions of the model were found to be in a good agreement with teeter angles measured during flight trials as it can be seen from Fig. 1 and 2. Table 1 summarizes the results of validation of *AMRA* model of blade teeter.

4.2. Validation of FEM Model of Blade Torsion

Deflections of beams of several lengths and with different torsional stiffness that were loaded statically by a torsional moment at the tip were computed by the *AMRA* FEM model of blade torsion. The results were then compared with analytical estimations of beam tip torsional deflections according to the St. Venant theory and were found to be in very good agreement. Mean relative deviation was less than 2%.

The shape of the first torsional mode predicted by the FEM model was also compared to corresponding torsional mode shapes that were published in open literature.[20] Predictions of the model are in good agreement with published data. Comparison of the first torsional mode shape computed by the FEM model of blade torsion with data published in open literature is depicted in Figure 3.

Since the span-wise distribution of blade torsion has a strong influence on blade aerodynamics, it is absolutely crucial that it is modelled correctly and the aerodynamic forcing of the blade is estimated realistically. Figures 4 and 5 depict a qualitative comparison of distribution of torque generated by rotor blade over the rotor disk as predicted by the *AMRA* model and qualitative sketch of torque distribution reproduced in open literature.[6]

Comparisons of the first natural frequencies in torsion and bending of two different rotor blades with results of experimental measurements and predictions of other models of blade dynamics represent another phase of *AMRA* validation. Data obtained during experimental measure-

ments of physical properties of the McCutcheon blade along with comprehensive data on physical properties of Aérospatiale SA330 Puma helicopter rotor blade were used.[24] A Southwell plot of the McCutcheon rotor blade is shown in Figure 6. Although first natural frequency in torsion is slightly under-predicted by the *AMRA*, general agreement with experimental data is good. Simple dynamic model of blade bending using spring stiffness and rigid blades was used during testing of the FEM model of blade torsion. Predictions of first natural frequency in bending of McCutcheon rotor blade is consistent with both theory and published shake tests of similar rotor blades.[25–28]

As it can be seen from Figure 7 predictions of first natural frequency in bending of Puma rotor blade is in reasonable agreement with results of *METAR/R85*. *CAMRAD* and *RAE/WHL* models predict lower values of the first natural torsional frequency than both *METAR/R85* and *AMRA*. Bousman *et al*[24], however, describes estimations of modal frequencies of *METAR/R85*, *CAMRAD* and *RAE/WHL* models as consistent.

4.3. Validation of FEM Model of Blade Bending

A coupled FEM model of blade torsion and bending was validated in similar manner as the FEM model of blade torsion. Predictions of both static and dynamic loading of the blade were compared with analytical predictions, experimental measurements and results of other structural analysis codes.

Predictions of static bending as obtained from the *AMRA* model are in good agreement with analytical predictions. Values of blade vertical displacement obtained with the model are roughly by 5% lower than analytical predictions and relative deviation of blade gradients is roughly 6% and these values do not change with loading, blade flexural stiffness or blade length.

Estimations of blade bending behaviour were validated against the same set of data that was used for validation of the FEM model of blade torsion.[24] The conclusion can be made that both static and dynamic behaviour of *AMRA* structural dynamics block was validated and that the model is likely to give realistic estimations of both rotor blade torsion and bending. Figures 8 and 9 depict distribution of torsional deflections and flexural vertical displacements over the rotor disk during forward flight.

5. Aeroelastic Stability of a Rotor in Autorotation

Unlike helicopter rotors, rotors in autorotation can experience significant variations in rotor speed during manoeuvres. Decrement of the rotor speed decreases centrifugal stiffness of the rotor and the resulting higher deflections in flap and twist generate more drag and may cause further drop in rotor speed. It is clear that thrust and torque of the rotor are functions of rotor speed and distribution of local angles of attack along the blade span. Further, angles of attack are dependent upon blade twist, rotor speed, descent rate and induced velocity. It can be easily shown that both descent rate and rotor angular velocity are strongly dependent upon rotor torque and rotor thrust. The *AMRA* model has shown that the extra degree of freedom in rotor speed has significant effect on the aeromechanics and aeroelastic stability of an autorotating rotor. A series of parametric studies that was carried out with the aid of the model[19] shows that blade induced twist (torsion), fixed angle of incidence of the blade and blade geometric twist have by far the strongest influence on the aeromechanical behaviour of a rotor in autorotation.

AMRA simulations were performed for three different levels of model complexity. The simplest configuration of the model used perfectly rigid rotor blades in both bending and torsion and blade flexibility was modelled with the aid of spring stiffness located at blade root. The second configuration of *AMRA* employed the FEM model of blade torsion while only spring stiffness was used for modelling of blade bending. The most complex variant of the model utilized coupled FEM models of both torsion and bending. Comparison of results obtained for these three model configurations allowed assessment of the effect of complexity of the structural dynamics model on performance and fidelity of *AMRA* simulations. In order to investigate rotor stability boundary in torsion, *AMRA* simulations for various values of torsional stiffness and chord-wise positions of centre of gravity (CG) were carried out.

The results of the simulations have revealed that low torsional stiffness of the blade leads to an aeroelastic instability (flutter) that manifests as coupled rotor speed / pitch / flap oscillations. These oscillations result in catastrophic decrease of rotor speed. This is a demonstration of strong rotor speed / pitch / flap coupling that exists only during autorotation. Decrement of the rotor speed decreases centrifugal stiffness

of the rotor and the resulting higher deflections in flap and twist generate more drag and cause further drop in rotor speed. This type of flutter is unique for rotors in autorotation since it differs from both helicopter rotor flutter and flutter of a fixed wing.

5.1. Aeroelastic Stability of a Rotor in Axial Autorotative Flight

Since blade aerodynamic forcing during steady axial autorotative flight is not dependent upon blade azimuth, it becomes constant after the rotor reaches equilibrium state. During steady vertical autorotation, overall torque generated by flow through the rotor disc is zero and rotor thrust is equal to the weight of the vehicle. The rotorspeed converges towards its steady value during torsional equilibrium. A characteristic span-wise distribution of blade torque for a rotor in the autorotative regime is observed. The inboard part of the blade generates positive torque and the outboard part of the blade generates negative torque.[5,6] The *AMRA* model describes all major features of aerodynamics of a rotor in autorotative axial descent very well.[19]

Results of the *AMRA* simulations obtained for different levels of complexity of the model show that torsion is the most important parameter to compute accurately; torsion therefore requires a FEM.

The aeroelastic behaviour of the rotor for two different levels of model complexity is shown in Fig.10 and 11. As it can be seen in the figures, reduction of rotor speed from a steady value to zero takes only few seconds. Speed of descent increases to unacceptable value during this time due to dramatic decrease of rotor thrust.

Parametric studies carried out with an earlier generation of the model (*AMRA*) and published in 32nd ERF proceedings[19] had shown that chord-wise position of CG seems to have much stronger influence on the stability of autorotation than chord-wise position of EA.

5.2. Aeroelastic Stability of a Rotor in Forward Autorotative Flight

Since autogyros operate mostly in the forward flight regime, modelling of forward autorotative flight represents the key task in investigation of aeroelastic behaviour of a autogyro rotor blade. Since both direction and value of the inflow velocity are functions of azimuth if horizontal speed is not zero there is no torque equilibrium during steady forward flight and the value of torque oscillates around the zero value. The amount of vibration induced by the rotor blade during steady forward flight is therefore significantly higher than in axial descent. In addition, free-stream velocity at the advancing side of the rotor disc is higher than at the retreating side, and thus the values of the forcing moments are higher and also asymmetrical.

Since aerodynamic forcing of the blade during steady forward flight has harmonic character, blade motion in both bending and torsion has harmonic components too. As in case of axial flight, simplification of the model of blade torsion seems to significantly degrade predictions of the model. Only small changes in behaviour are seen when bending is modelled by an equivalent spring stiffness rather than a FEM.

Similarly as in case of axial flight in autorotation, simulations for various torsional stiffness and chord-wise positions of centre of gravity were performed. Computations carried out with the aid of the *AMRA* model have shown that the rotor suffers of aeroelastic instability if CG lies aft EA. Aeroelastic behaviour of the rotor for all three different levels of model complexity has very similar character to the aeroelastic instability predicted in autorotative vertical descent and it is shown in Fig.12 and 13. The resulting aeroelastic stability boundary can be found in Fig.14. It can be seen from the figure that position of CG aft EA is destabilizing, similar to fixed wing classical flutter and helicopter pitch flap flutter.

6. Conclusions

An aeromechanical model of a autogyro rotor *AMRA* was developed in the MATLAB programming language and used in predicting the aeroelastic behaviour of a rotor. Two regimes were investigated - autorotative axial flight (vertical descent) and forward flight in autorotation. Simulations have shown that autorotation is a complex aeromechanical process with auto-stabilizing characteristics. In order to obtain input parameters for the structural model of the blade, a series of experimental measurements were carried out on a typical autogyro blade. Blade mass distribution, position of elastic axis, span-wise distribution of CG and torsional and flexural stiffness was determined during the experiments.

Results from the AMRA model were verified and found to be in reasonable agreement with experimental measurements. Several paramet-

ric studies were performed so as to gain more knowledge on the effect of blade geometry and structural properties on performance of the rotor during autorotation.

It was found that blade twist / bending / rotor speed coupling has major effect on the stability of autorotation when the rotor is in a stable configuration. Computations were performed for three different levels of complexity of the model of blade structural dynamics. Results of the *AMRA* simulations have shown that detailed modelling of rotor blade torsion (i.e. blade induced twist) has major influence on aeromechanics of a rotor in autorotation. It was shown in the paper that it is sufficient to model only first bending mode, i.e. to assume constant span-wise distribution of flap angle. The conclusion can be made that any aeroelastic simulation of a rotor in autorotation should contain model that gives realistic predictions of blade dynacmics in torsion.

Occurrence of a type of flutter that is unique for autorotating rotors was predicted by the model both during axial descent in autorotation and autorotative forward flight. This aeroelastic instability is driven by blade pitch / bending / rotor speed coupling and differs from both flutter of a helicopter rotor and flutter of a fixed wing. The instability results in catastrophic decrease of the rotor speed and significant increase of speed of descent.

Acknowledgments

The authors would like to acknowledge the continued support for autogyro research provided by the UK Civil Aviation Authority. This work is funded through a CAA ARB Fellowship. The support and advise from Steve Griffin, Jonathan Howes, Alistair Maxwell, Andrew Goudie and Joji Waites is highly appreciated. Many thanks go also to Dr Richard Green and the departmental team of technicians from Acre Road laboratories for help with the experimental measurements.

References

1. Thomson, D.G., Houston, S.S., Spathopoulos, V. M., *Experiments in Autogiro Airworthiness for Improved Handling Qualities*, Journal of American Helicopter Society, Pg. 295, No. 4, Vol. 50, October 2005.

2. Houston, S. S., *Longitudinal Stability of Autogyros*, The Aeronautical Journal, Vol. 100 (991), 1996, pp. 1-6.

3. Houston, S. S., *Identification of Autogiro Longitudinal Stability and Control Characteristics*, Journal of Guidance, Control and Dynamics, Vol. 21, No. 3, 1998, pp. 391-399.

4. Coton, F., Smrcek, L., Patek, Z., *Aerodynamic Characteristics of a autogyro Configuration*, Journal of Aircraft, Vol. 35, No. 2, 1998, p. 274 - 279.

5. Leishman, J.G., *The Development of the Autogiro: A Technical Perspective*, Journal of Aircraft, Vol. 41, (2), 2004, pp. 765-781.

6. Leishman, J.G., *Principles of Helicopter Aerodynamics*, Cambridge University Press, 2nd Edition, 2006, ISBN 0-521-85860-7.

7. Prouty, R. W., *Helicopter Performance, Stability and Control*, Robert E. Krieger Publishing Co., Malabar, FA, USA, 1990.

8. Sheldahl, R. E., Klimas, P. C., *Aerodynamic Characteristics of Seven Aerofoil Sections Through 180 Degrees Angle of Attack for Use in Aerodynamic Analysis of Vertical Axis Wind Turbines*, SAND80-2114, Sandia National Laboratories, Albuquerque, New Mexico, USA, 1981.

9. Nikolsky, A.A., Seckel, E., *An Analytical Study of the Steady Vertical Descent in Autorotation of Single-Rotor Helicopters*, NACA TN 1906, Washington, 1949.

10. Wheatley, B., Bioletti, C., *Wind-Tunnel Tests of a 10-foot-diameter autogyro Rotor*, NACA TR 536.

11. Wheatley, J.B., *The Aerodynamic Analysis of the autogyro Rotating-Wing System*, NACA TN 492, Langley Memorial Aeronautical Laboratory, 1934.

12. Wheatley, J.B., *An Aerodynamic Analysis of the Autogiro Rotor with a Comparison between Calculated and Experimental Results*, NACA TR 487, 1934.

13. Carpenter, P.J., *Lift and Profile-drag Characteristics of an NACA 0012 Airfoil Section as Derived from Measured Helicopter-rotor Hovering Performance*, NACA TN 4357, Langley Memorial Aeronautical Laboratory, Langley Field, VA, USA, 1958.

14. *www.cyberiad.net/foildata.htm*, visited in the fall 2005

15. Houston, S. S., *Modelling and Analysis of Helicopter Flight Mechanics in Autorotation*, Journal of Aircraft, Vol. 40, No. 4, 2003.

16. Chen, R. T. N., *A Survey of Nonuniform Inflow Models for Rotorcraft Flight Dynamics and Control Applications*, NASA TM 102219, Ames Research Centre, California, USA, 1989.

17. Houston, S. S., Brown, R. E., *Rotor Wake Modelling for Simulation of of Helicopters Flight Mechanics in Autorotation*, Journal of Aircraft, Vol. 40, No. 5, 2003.

18. Bramwell, A. R. S. et al, *Bramwell's Helicopter Dynamics*, Second edition, Butterworth-Heinemann, 2001. ISBN 0-7506-5075-3

19. Trchalík, J., Gillies, E.A., Thomson, D.G., *Aeroelastic Behaviour of a gyroplane Rotor in Axial Descent and Forward Flight*, 32nd European Rotorcraft Forum, Maastricht, Netherlands, October 2006.

20. Bielawa, R. L., *Rotary Wing Structural Dynamics and Aeroelasticity*, Second edition, AIAA Education series, 2006. ISBN 1-56347-698-3

21. Kwon, Y. W., Bang, H., *The Finite Element Method Using MATLAB*, Second Edition, CRC Press, 2000, ISBN 0-8493-0096-7.

22. Houston, S.S., *Validation of a Rotorcraft Mathematical Model for Autogyro Simulation*, AIAA Journal of Aircraft, Vol. 37, No. 3, pp. 203-209, 2000.

23. Bagiev, M., *Autogyro Handling Qualities Assessment Using Flight Testing and Simulation Techniques*, PhD Thesis, Dept. of Aerospace Engineering, University of Glasgow, 2005.

24. Bousman, W.G., Young, C., Toulmany, F., Gilbert, N.E., Strawn, R.C., Miller, J.V., Maier, T.H., Costes, M., *A Comparison of Lifting-Line and CFD Methods with Flight Test Data from a Research Puma Helicopter*, NASA TM 110421, Ames Research Center, Moffett Field, CA, USA, 1996.

25. Friedman, P. P., *Rotary-Wing Aeroelasticity: Current Status and Future Trends*, AIAA Journal, Vol. 42, No. 10, October 2004.

26. Friedman, P. P., Hodges, D.H., *Rotary Wing Aeroelasticity - A Historical Perspective*, Journal of Aircraft, Vol. 40, No. 6, November-December 2003.

27. Wilkie, W.K., Mirick P.H., Langston, Ch.W., *Rotating Shake Test and Modal Analysis of a Model Helicopter Rotor Blade*, NASA TM 4760, ARL TR 1389, Langley Research Center, Hampton, VA, USA, 1997.

28. Maier, T.H., Sharpe, D.L., Abrego, A.I., *Aeroelastic Stability for Straight and Swept-Tip Rotor Blades in Hover and Forward Flight*, AHS 55th Annual Forum, Montreal, Quebec, Canada, 1999.

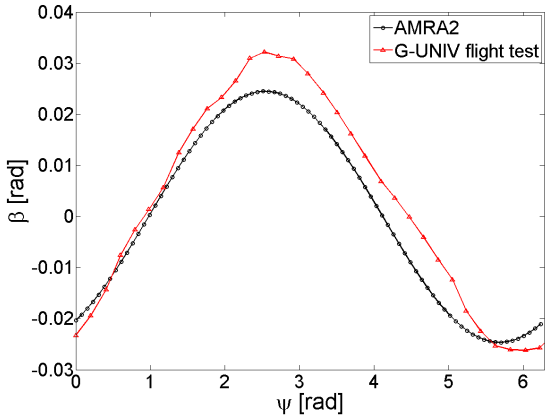

Figure 1: *Comparison of predictions of rotor blade teeter and G-UNIV experimental data*

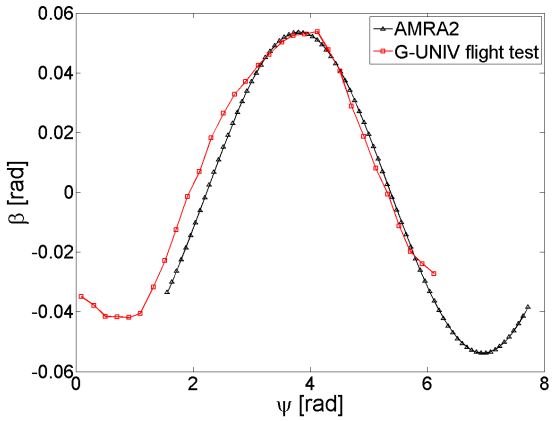

Figure 2: *Comparison of predictions of rotor blade teeter and G-UNIV experimental data*

Table 1: *Comparison of predictions of rotor blade teeter and G-UNIV experimental data*

CASE	V_H	Ω	β exp	β AMRA
	[m/s]	[rad/s]	[rad]	[rad]
A	14	38	0.031	0.026
B	27	41	0.058	0.056

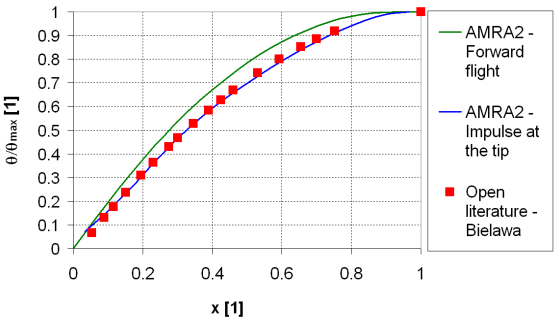

Figure 3: *Comparison of the first torsional mode shape computed by the* AMRA *and published data*

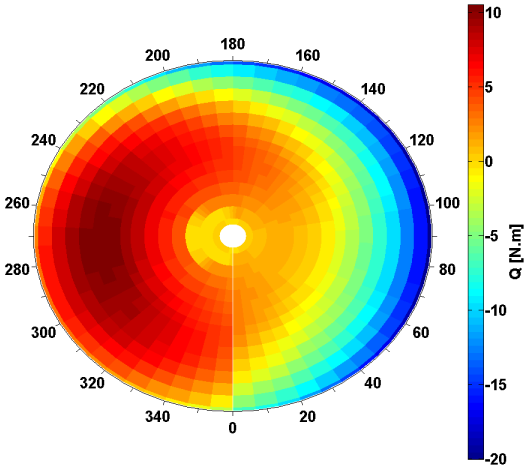

Figure 4: *Distribution of blade torque over rotor disk during steady forward flight in autorotation estimated by* AMRA

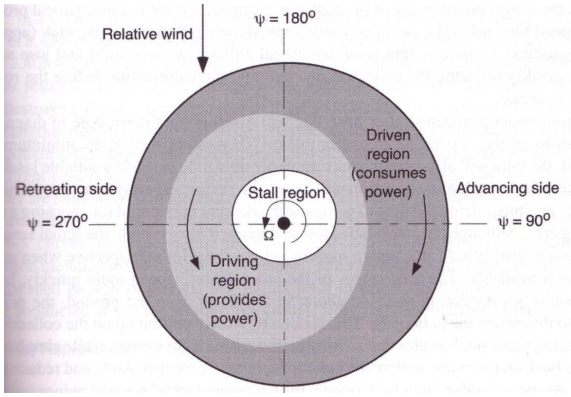

Figure 5: *Distribution of blade torque over rotor disk during steady forward flight in autorotation published by Leishman*[6]

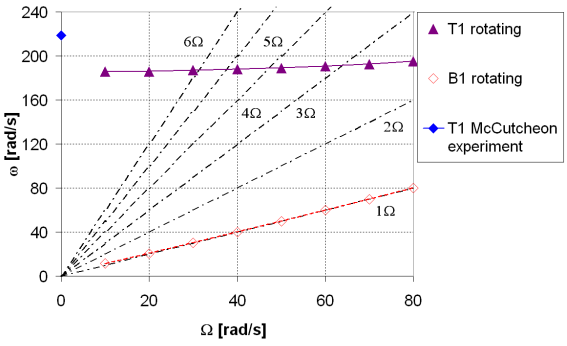

Figure 6: *Southwell plot of McCutcheon rotor blade showing correct qualitative behaviour.*

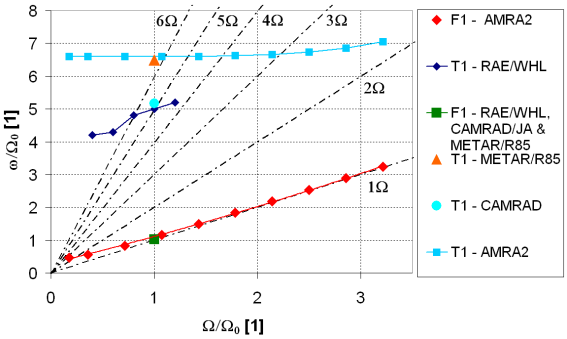

Figure 7: *Southwell plot Aérospatiale SA330 Puma helicopter rotor blade showing correct qualitative behaviour. Data in the plot are non-dimensionalised with* $\Omega_0 = 28 rad/s$.

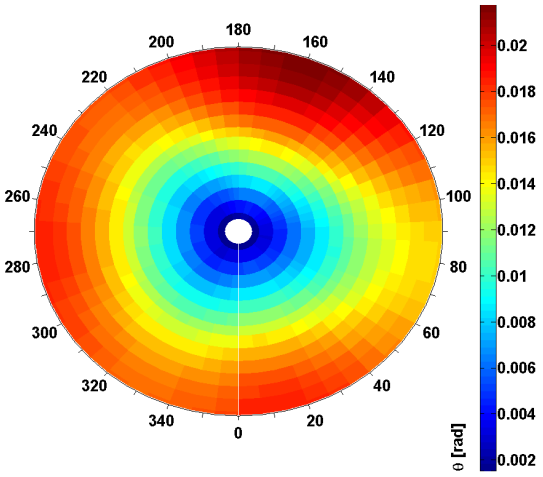

Figure 8: *Distribution of blade torsional deflection obtained with the aid of* AMRA.

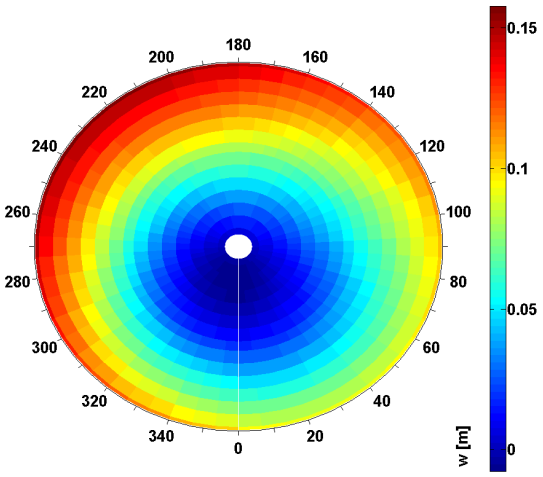

Figure 9: *Distribution of blade vertical displacement in bending obtained with the aid of* AMRA.

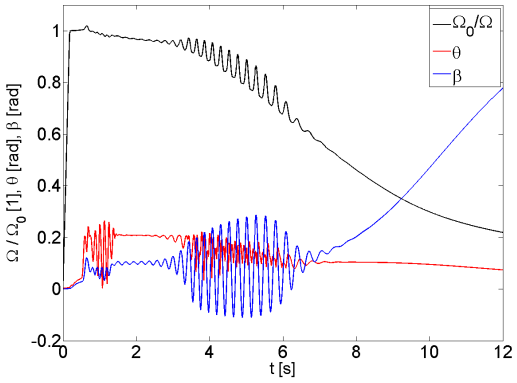

Figure 10: *An example of an aeroelastic instability during axial flight in autorotation as predicted by the* AMRA. *The data shown in the plot were acquired with the aid of simplified model of blade dynamics that is using equivalent spring stiffness for modelling both torsion and bending. Calculated for the value of blade torsional stiffness of* $100 N.m^2/rad$, *elastic axis at 32% of blade chord and blade centre of gravity at 40% of blade chord.*

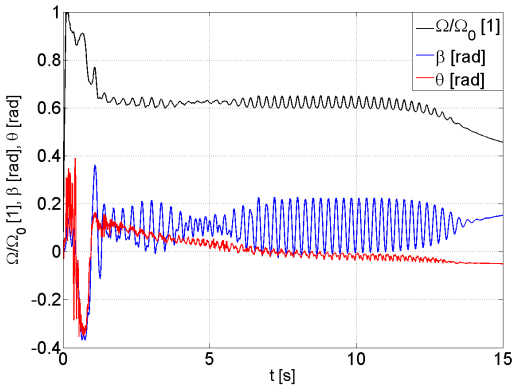

Figure 11: *An example of an aeroelastic instability during axial flight in autorotation as predicted by the* AMRA. *Coupled FEM model of blade torsion and bending was used. Calculated for the value of blade torsional stiffness of* $400 N.m^2/rad$, *elastic axis at 32% of blade chord and blade centre of gravity at 40% of blade chord.*

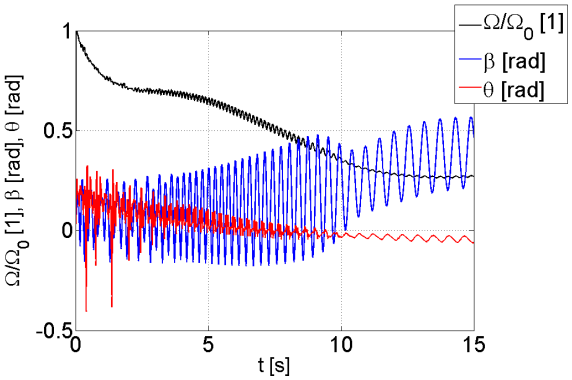

Figure 12: *An example of an aeroelastic instability during forward flight in autorotation as predicted by the* AMRA. *The data shown in the plot were acquired with the aid of simplified model of blade dynamics that is using equivalent spring stiffness for modelling both torsion and bending. Calculated for the value of blade torsional stiffness of* $300 N.m^2/rad$, *elastic axis at 32% of blade chord and blade centre of gravity at 40% of blade chord.*

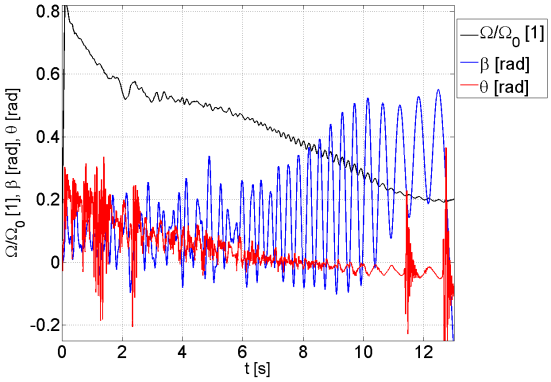

Figure 13: *An example of an aeroelastic instability during forward flight in autorotation as predicted by the* AMRA. *Coupled FEM model of blade torsion and bending was used. Calculated for the value of blade torsional stiffness of* $600 N.m^2/rad$, *elastic axis at 32% of blade chord and blade centre of gravity at 40% of blade chord.*

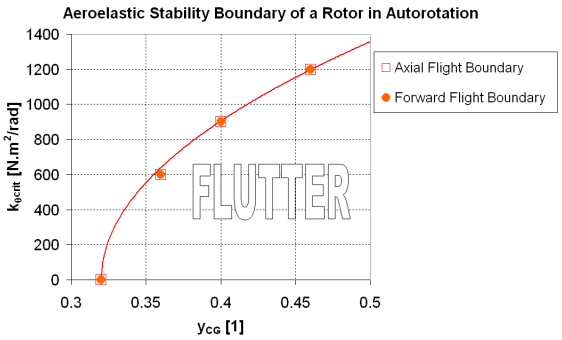

Figure 14: *Stability boundary for autorotative flight*